Aeroelastic Tailoring of Aft-Swept High-Aspect-Ratio Composite Wings

John A. Green*
Stanford University, Stanford, California

The integrating matrix method is used to study the aeroelastic performance of aft-swept high-aspect-ratio wings. Aeroelastic stability boundaries are shown as a function of fiber angle and dimensionless modulus parameters for straight wings of aspect ratio 14. Certain laminates show divergence for wings with low sweep angles, but for most laminates and wing sweeps, flutter was the instability. The bending-torsion coupling that is beneficial for forward-swept wings is shown to be of no advantage for aft-swept wings, for which torsional stiffness is much more significant. Both symmetric and nonsymmetric ply orientations were studied, and it is demonstrated that there need not be a severe penalty for using general laminates.

Nomenclature

A_{ij}, a_{ij} = extensional modulus/compliance
a.c. = location of aerodynamic center in semichords, positive aft of midchord
B_{ij}, b_{ij} = nonsymmetric coupling modulus/compliance
b_R = structural semichord
$c_{l\alpha}$ = lift-curve slope
c_R = aerodynamic chord
D_{ij}, d_{ij} = bending modulus/compliance
e = location of structural axis in semichords, positive aft of midchord
l = semispan
M = mass matrix
M_x, M_{xy} = dimensionless bending moments
M_α, M_w, M_γ = dimensionless aerodynamic moments
$m_{i,j}$ = dimensionless mass terms
m_R = mass per unit length at root
Q_{ij} = transformed modulus
q, q^* = dimensional/normalized dynamic pressure; $q^* = q/q_{\text{ref}}$
$\bar{q}$ = dimensionless dynamic pressure, $= \rho b_R l^3 V^2 \cos^2\Lambda / c_R D_{11_R}$
R = dimensionless bending-torsion ratio
r_α = dimensionless radius of gyration
s = dimensionless Laplace variable
V = velocity
V_x = dimensionless transverse shear force
w = vertical displacement
x, y = dimensionless spanwise, chordwise coordinate
Z = matrix of dimensionless structural compliances
α = angle of attack
γ = bending rotation angle
θ = laminate ply orientation angle
Λ = sweep angle
μ = mass ratio, $= m_R/\pi\rho b_R^2$
ρ = air density
χ_α = dimensionless static unbalance relative to structural axis, positive aft
ψ, ψ_i = dimensionless coupling parameters

Subscripts and Superscripts

D = displacement variable
F = force variable
R = value at wing root
ref = reference value
S = symmetric laminate
T = total laminate
$(\hat{\ })$ = global matrix or vector

Introduction

THE concept of aeroelastic tailoring has brought renewed interest to forward-swept wings, and, consequently, this configuration has been the focus of much of the research on the subject. The recent survey paper by Shirk et al.[1] cites many studies of aircraft with forward-swept wings, but relatively few dealing with high-aspect-ratio aft-swept configurations. This is quite understandable, since the first application of the concept was for the elimination of divergence of forward-swept wings.[2] Weisshaar and Ryan[3] considered the effects of tailoring both forward- and aft-swept wings, but in a quite general manner.

However, future transport aircraft are certain to make use of composite materials in their primary structures and are likely to have quite high aspect ratios.[4] A high-aspect-ratio aft-swept wing is less prone to aeroelastic divergence, but the increase in aspect ratio could cause flutter to become a problem. One of the few papers devoted solely to the problem of tailoring high-aspect-ratio composite wings is the work by Gimmestad,[5] but this is limited to some simple cases. A further area of aeroelastic tailoring that has received relatively little attention is in the use of nonsymmetric laminates. This research considers the use of both symmetric and nonsymmetric laminates to improve the aeroelastic performance of high-aspect-ratio aft-swept wings.

This problem is solved using an integrating matrix method, which was used by Lehman[6,7] to analyze some simple aeroelastic examples and by Green[8] to study the effects of stores on forward-swept wings. The method requires the fourth-order differential equation for flutter to be written in a state vector form, and then an integrating matrix is applied to the resulting first-order matrix equation, which is then solved iteratively. Although this is a numerical solution method, it requires only a small number of elements (typically four or five) to obtain a converged solution. The main advantage of the integrating matrix method is that, because it requires only a small number of elements, a large number of parameters can be investigated. Clearly, the choice of layup of the fibers is fundamental to the design process, and this forms the bulk of the research.

Received Nov. 25, 1986; revised April 28, 1987.

*Research Assistant, Aeronautics and Astronautics. Student Member AIAA.

Solution of the Aeroelastic Equations

State Vector Formulation

The aeroelastic behavior of the wing shown in Fig. 1 may be represented as a fourth-order differential equation, and the integrating matrix technique is applied to this equation to obtain a solution. An outline of the general method is given here, and a more detailed treatment can be found in Ref. 7.

In order to apply the integrating matrix method, the equation of motion must first be written in a state vector form. The fourth-order differential equation is written in terms of a state vector, y, comprised of four displacement and four force degrees of freedom,

$$\frac{d}{dx}\begin{Bmatrix} N_x \\ M_x \\ V_x \\ M_{xy} \\ u \\ \gamma \\ w \\ \alpha \end{Bmatrix} = \begin{bmatrix} 0 & 0 & 0 & 0 & 0 & 0 & 0 & 0 \\ 0 & 0 & 1 & 0 & 0 & 0 & 0 & 0 \\ 0 & 0 & 0 & 0 & 0 & 0 & 0 & 0 \\ 0 & 0 & 0 & 0 & 0 & 0 & 0 & 0 \\ a_{11} & b_{11} & 0 & b_{16} & 0 & 0 & 0 & 0 \\ b_{11} & d_{11} & 0 & d_{16} & 0 & 0 & 0 & 0 \\ 0 & 0 & 0 & 0 & 0 & -1 & 0 & 0 \\ b_{16} & d_{16} & 0 & d_{66} & 0 & 0 & 0 & 0 \end{bmatrix} \begin{Bmatrix} N_x \\ M_x \\ V_x \\ M_{xy} \\ u \\ \gamma \\ w \\ \alpha \end{Bmatrix}$$

$$+s^2 \begin{bmatrix} 0 & 0 & 0 & 0 & 0 & 0 & 0 & 0 \\ 0 & 0 & 0 & 0 & 0 & 0 & 0 & 0 \\ 0 & 0 & 0 & 0 & 0 & 0 & m_{ww} & m_{w\alpha} \\ 0 & 0 & 0 & 0 & 0 & 0 & m_{w\alpha} & m_{\alpha\alpha} \\ 0 & 0 & 0 & 0 & 0 & 0 & 0 & 0 \\ 0 & 0 & 0 & 0 & 0 & 0 & 0 & 0 \\ 0 & 0 & 0 & 0 & 0 & 0 & 0 & 0 \\ 0 & 0 & 0 & 0 & 0 & 0 & 0 & 0 \end{bmatrix} \begin{Bmatrix} N_x \\ M_x \\ V_x \\ M_{xy} \\ u \\ \gamma \\ w \\ \alpha \end{Bmatrix}$$

$$- \begin{bmatrix} 0 & 0 & 0 & 0 & 0 & 0 & 0 & 0 \\ 0 & 0 & 0 & 0 & 0 & 0 & 0 & 0 \\ 0 & 0 & 0 & 0 & 0 & L_\gamma & L_w & L_\alpha \\ 0 & 0 & 0 & 0 & 0 & M_\gamma & M_w & M_\alpha \\ 0 & 0 & 0 & 0 & 0 & 0 & 0 & 0 \\ 0 & 0 & 0 & 0 & 0 & 0 & 0 & 0 \\ 0 & 0 & 0 & 0 & 0 & 0 & 0 & 0 \\ 0 & 0 & 0 & 0 & 0 & 0 & 0 & 0 \end{bmatrix} \begin{Bmatrix} N_x \\ M_x \\ V_x \\ M_{xy} \\ u \\ \gamma \\ w \\ \alpha \end{Bmatrix} \quad (1)$$

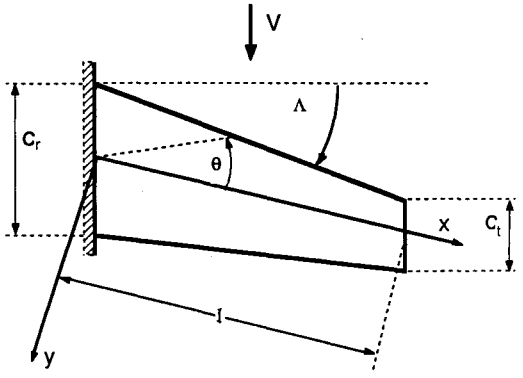

Fig. 1 Geometric layout of wing.

or

$$y' = Zy + s^2 My - Q(s,\bar{q})y \quad (2)$$

The structural matrix Z is derived from an anisotropic plate beam model[9] and contains the compliances required for bending, torsion, and extension of a beam. Transverse shear effects are neglected, and free warping of the cross section at the root is assumed. Although warping restraint would not be expected to have a large influence on a high-aspect-ratio isotropic wing, Librescu and Simovich[10] have shown that, for composite wings, warping restraint is a more complex issue. The compliances are computed from the inverse of the modulus matrix, for which the moduli are given by

$$A = \int_{-h/2}^{h/2} Q_{ij}\,dz = h_0 \sum_{r=1-n/2}^{n/2} Q_{ij}^r [r-(r-1)]$$

$$B = \int_{-h/2}^{h/2} Q_{ij} z\,dz = \frac{h_0^2}{2} \sum_{r=1-n/2}^{n/2} Q_{ij}^r [r^2-(r-1)^2]$$

$$D = \int_{-h/2}^{h/2} Q_{ij} z^2\,dz = \frac{h_0^3}{3} \sum_{r=1-n/2}^{n/2} Q_{ij}^r [r^3-(r-1)^3] \quad (3)$$

The terms Q_{ij} are the transformed moduli for each lamina and are dependent on the fiber orientation angle θ. These moduli are then integrated through the laminate, and if all layers have the same thickness (h_0) the integration is replaced by the sum shown in Eq. (3). It should be noted that, if the lamina are arranged symmetrically with respect to the midline, there is no contribution to the B_{ij} terms, which can be dropped from the analysis. In such a case, the N_x and u terms may be omitted, and this reduces the order of the system from 8×8 to 6×6. The following development describes the nonsymmetric case, and the development using the reduced-order system is found in Refs. 6–8.

The aerodynamic matrix Q contains dimensionless lift and moment terms derived from modified strip theory,[11] for which the time dependence is based on Jones' approximation to the Theodorsen function

$$C(s) = \frac{0.5s^2 + 0.2808s + 0.01365}{s^2 + 0.3455s + 0.01365} \quad (4)$$

One feature of the modified strip theory is that the section lift-curve slope $c_{l\alpha}$ may also be varied along the span.

Application of the Integrating Matrix

The integrating matrix technique is a numerical method that requires that the wing be divided into $n-1$ elements with n nodes. Thus, each term in the state vector becomes a vector of order n, and the concept of a global state vector $\hat{y}$

is introduced to represent the discrete version of the problem. Similarly, there will be global matrices $\hat{Z}$, $\hat{M}$, and $\hat{Q}$ comprised of $n \times n$ block diagonal matrices Z, M, and Q.

The global integrating matrix $\hat{L}$ is now defined as

$$\hat{L} \equiv \begin{bmatrix} L & \cdots & 0 \\ \vdots & \ddots & \vdots \\ 0 & \cdots & L \end{bmatrix} \tag{5}$$

where L is the local integrating matrix. The local integrating matrix is, in fact, the product of a summing matrix and a weighting matrix based on Jacobi polynomials. Tables of the Jacobi integrating matrices are given in Ref. 7.

$\hat{L}$ has the effect of integrating the derivative on the left-hand side of Eqs. (1) and (2) and reducing the integration on the right-hand side to simple matrix multiplication. Thus, the integrated form of Eq. (2) is

$$\hat{y} = \hat{L}\hat{Z}\hat{y} + s^2\hat{L}\hat{M}\hat{y} - \hat{L}\hat{Q}(s,\bar{q})\hat{y} + \hat{k} = \hat{L}[\hat{Z}\hat{y} + \hat{A}\hat{y}] + \hat{k} \tag{6}$$

with the following definition introduced for conciseness:

$$\hat{A} \equiv s^2\hat{M} - \hat{Q}(s,\bar{q}) \tag{7}$$

$\hat{k}$ is a vector of the constants of integration determined from the boundary conditions.

Boundary Conditions

The choice of boundary condition is of fundamental importance because the condition applied affects both the complexity and accuracy of the solution. A cantilever condition is the simplest to apply, and was used in many of the early studies of aeroelastic tailoring. Although the use of such a condition precludes the detection of body freedom flutter,[12,13] it is used here to avoid the appearance of nonhomogeneous boundary condition terms.

First, it is necessary to define a global boundary condition matrix $\hat{B}$ having the following properties:

$$\hat{B}\hat{y} = 0, \qquad \hat{B}\hat{k} = \hat{k} \tag{8}$$

This global matrix is once again comprised of blocks of local boundary condition matrices, one for each of the variables. If both sides of Eq. (6) are multiplied by $\hat{B}$, and the properties of Eq. (8) are used, it is possible to solve for $\hat{k}$.

$$\hat{k} = -\hat{B}[\hat{L}(\hat{Z}\hat{y} + \hat{A}\hat{y})] - \hat{B}_{nh}\hat{y} \tag{9}$$

$\hat{B}_{nh}$ is a second boundary condition matrix, which accounts for any nonhomogenous boundary conditions. This matrix is null for the cantilever case, but if rigid-body modes are included it becomes nonzero, and this significantly complicates the solution.

In general, a cantilever boundary condition requires that there be no displacement at the root and no force at the tip, thus

$$u(0) = 0, \quad \gamma(0) = 0, \quad w(0) = 0, \quad \alpha(0) = 0 \tag{10}$$

$$N_x(1) = 0, \quad M_x(1) = 0, \quad V_x(1) = 0, \quad M_{xy}(1) = 0 \tag{11}$$

An equation for each of the state variables is obtained by expansion of Eq. (6), and the boundary conditions are then applied to each variable in turn. This gives the constants of integration in a form that may be compared to Eq. (10), which in turn allows the boundary condition matrix $\hat{B}$ to be determined. For a cantilever boundary condition, this matrix is very simple, containing only ones and zeros.

Equation Reduction

The problem is now in a position to be solved, since Eq. (9) can be substituted into Eq. (6), and collecting terms allows the equation to be written as

$$[\hat{H} + \hat{F}\hat{A}]\hat{y} = 0 \tag{12}$$

where

$$\hat{F} \equiv [\hat{B} - \hat{I}]\hat{L}, \qquad \hat{H} \equiv [\hat{I} + \hat{F}\hat{Z} + \hat{B}_{nh}] \tag{13}$$

Since the state vector consists of force and displacement components, it can be written in partitioned form as

$$\left(\begin{bmatrix} H_{FF} & 0 \\ H_{DF} & H_{DD} \end{bmatrix} + \begin{bmatrix} 0 & F_{FF}A_{FD} \\ 0 & 0 \end{bmatrix} \right) \begin{Bmatrix} y_F \\ y_D \end{Bmatrix} = \begin{Bmatrix} 0 \\ 0 \end{Bmatrix} \tag{14}$$

This equation can be solved simultaneously to eliminate the force variable y_F which gives

$$[I + TA_{FD}]y_D = 0 \tag{15}$$

where

$$T = -H_{DD}^{-1}H_{DF}H_{FF}^{-1}F_{FF} \tag{16}$$

The matrix T contains structural information and information from the boundary conditions; A_{FD} contains the aerodynamic and mass properties of the wing. Since the problem is now written in terms of only one-half of the original state vector, the system of equations is reduced in size by a factor of 4, and solution is much faster.

Substitution of the boundary condition matrix into Eq. (13) allows analytical inversion of H_{DD}^{-1} and H_{FF}^{-1}. This, in turn, permits expressions for T to be formed:

$$T = \begin{bmatrix} La_{11}L_1 & Lb_{11}L_1 & -Lb_{11}L_1^2 & Lb_{16}L_1 \\ Lb_{11}L_1 & Ld_{11}L_1 & -Ld_{11}L_1^2 & Ld_{16}L_1 \\ -L^2b_{11}L_1 & -L^2d_{11}L_1 & L^2d_{11}L_1^2 & -L^2d_{16}L_1 \\ Lb_{16}L_1 & Ld_{16}L_1 & -Ld_{16}L_1^2 & Ld_{66}L_1 \end{bmatrix} \tag{17}$$

with

$$L_1 \equiv (B_n - I)L \tag{18}$$

where B_n is a matrix of zeros except in the nth column, which contains ones.

Solution Procedure

Equation (15) has a solution if

$$\det |I + TA_{FD}(s,\bar{q})| = 0 \tag{19}$$

For each value of dynamic pressure $\bar{q}$, Eq. (19) is solved iteratively to find the value of the Laplace variable s, which makes the determinant zero. Muller's method[14] is an efficient root-solving scheme that will find the roots of a complex matrix equation, and this is employed in the solution procedure.

One useful property of the cantilever boundary condition is that the T matrix is independent of both $\bar{q}$ and s, so for a particular wing geometry it can be evaluated before beginning the iteration procedure. This is not so when rigid-body modes are included, because, in that case, T contains terms that depend on $\bar{q}$ and s. This requires that the matrix be recalculated for each iterate, which consequently increases the time needed for computational solution.

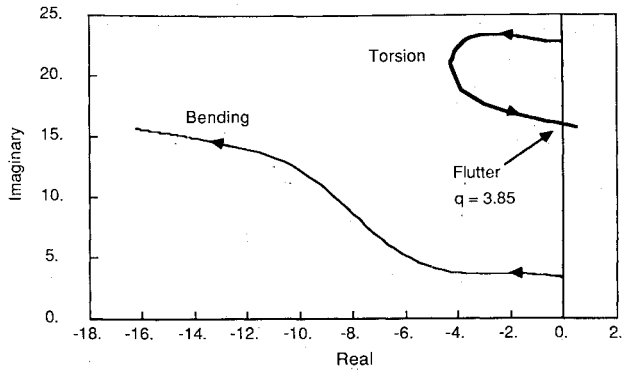

Fig. 2 Root locus of reference flutter root: $\mathcal{R}=14$, $\Lambda=0$ deg, $\theta=0$ deg.

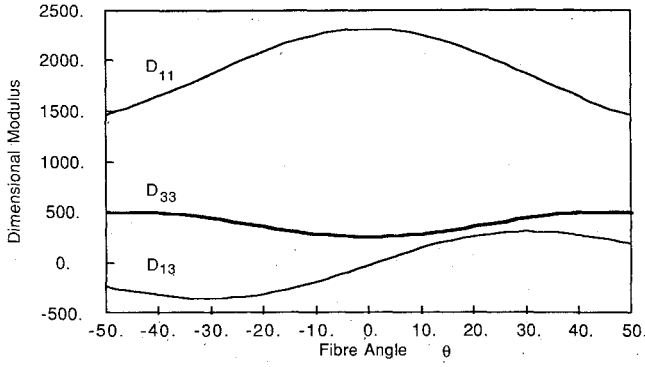

Fig. 3a Dimensional moduli as a function of fiber angle θ for reference laminate.

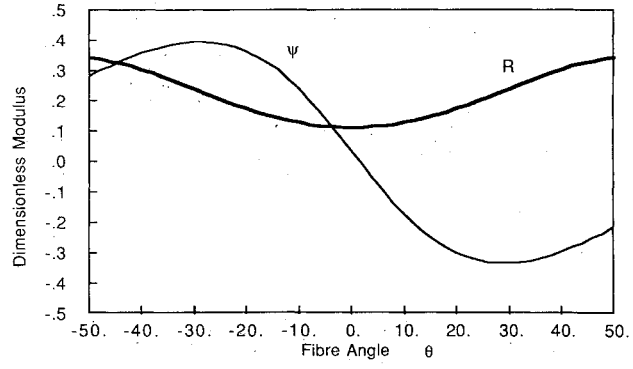

Fig. 3b Dimensionless modulus parameters as a function of fiber angle θ for reference laminate.

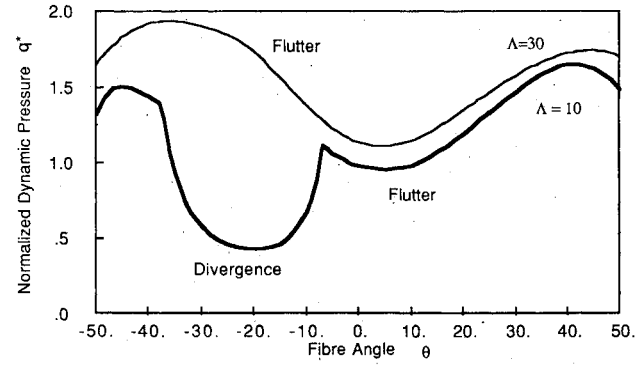

Fig. 4 Aeroelastic stability boundary for reference laminate.

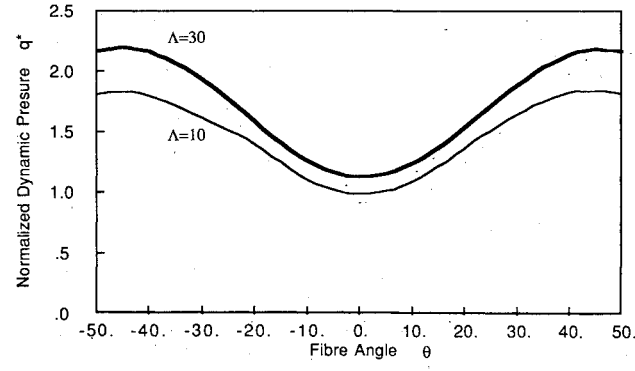

Fig. 5a Aeroelastic boundary for $\theta_1=\theta$ and $\theta_2=-\theta$.

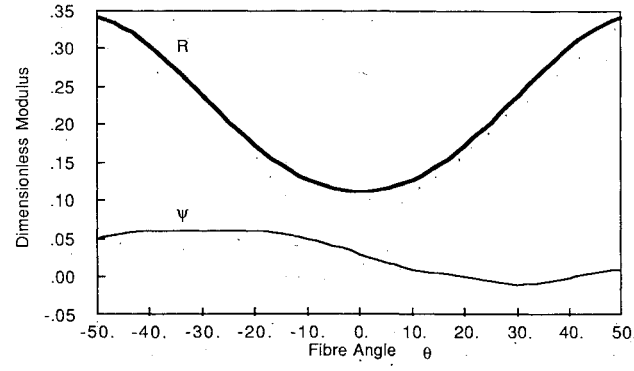

Fig. 5b Dimensionless modulus parameters R and ψ for $\theta_1=\theta$ and $\theta_2=-\theta$.

In order to determine the dynamic pressure at which aeroelastic instability occurs, the roots of Eq. (19) are traced out for increasing values of $\bar{q}$ until one of the roots crosses the imaginary axis. Thus, a root locus in the s plane can be produced (Fig. 2), which will indicate when an aeroelastic instability has occurred and whether it is flutter or divergence. If the vibration frequencies of the wing are also known and identified as being bending or torsion modes, it is possible to determine the type of flutter. The dimensionless flutter dynamic pressure shown in Fig. 2 is the reference flutter pressure used to normalize the remaining figures.

It is not necessary to trace out a root locus for each configuration, and a procedure was devised to find the dynamic pressure at which an instability occurs using a secant algorithm. This procedure efficiently locates the dynamic pressure at which the root locus crosses the imaginary axis and indicates the type of aeroelastic instability.

Numerical Stability

As with any numerical method, some attention must be given to convergence. The choice of the number of nodes to be used is important for reasons of both speed and accuracy. As mentioned earlier, the size of the determinant to be solved is $3n\times3n$ or $4n\times4n$ and, since the determinant is solved iteratively, the speed at which the calculations are made is highly dependent on the number of nodes.

Table 1 shows dimensionless dynamic pressure values for flutter of a straight wing and one with a taper ratio of 0.25. The number of nodes is varied from 3 to 6, and the relative computational time needed for solution using an IBM 3084 computer is shown. For the straight wing, convergence is very good, with the difference between the four- and six-node solution being 0.24%. However, when the wing is tapered, six nodes are needed for the solution to be reasonably well converged. This is because the taper of the

wing has to be treated in a discrete manner, and more nodes are needed to reflect the additional information. For the remaining results, four nodes were used to keep computational time to a minimum.

Results

The remainder of this analysis presents results for a reference laminate, and several different ply orientations, including nonsymmetric laminates, with the effects of both ply orientation and modulus shown. Although the integrating matrix method is capable of analyzing tapered configurations with the variable $c_{l\alpha}$, this adds to the computational time needed, and, since these effects would not be expected to alter the trends, they are not included in this study.

In much of the literature on aeroelastic tailoring, either the ply orientation or the modulus is given, but seldom both. An understanding of the effects of both are of importance to the designer; thus, the results presented show the aeroelastic stability boundary as a function of a reference ply angle (θ) and also the dimensionless modulus as a function of the same ply angle. This allows the effect of ply angle on both stability and modulus to be considered. Following Weisshaar and Ryan,[3] the moduli are made dimensionless in the following manner:

$$R=\frac{D_{66}}{D_{11}},\quad \psi=\frac{-D_{16}}{\sqrt{D_{11}D_{33}}},\quad \psi_1=l\frac{B_{11}}{D_{11}},\quad \psi_2=l\frac{B_{16}}{D_{66}} \tag{20}$$

The extensional coupling moduli need to be multiplied by a characteristic length—in this case, the semispan l—to become dimensionless. The use of the moduli in dimensionless form makes the results more general.

Reference Laminate

The design of an aircraft involves many variables, and the use of composite materials increases the complexity of the design problem. The integrating matrix method is a useful tool for preliminary design work because it is not only fast, but also capable of modeling fairly sophisticated effects. In this section, results are presented for a reference case, with the properties shown in Table 2.

The laminate code for this reference case is given by

$$[\theta,\theta,0,0,\mp 45,0,\mp 45,0,\mp 45]_s \tag{21}$$

where θ is the reference fiber orientation angle. For this first part of the study, the outermost plies on both the top and bottom surfaces of the wing are varied as a group between -50 and 50 deg. The bending, torsional, and coupling moduli are shown in Fig. 3a, and the equivalent dimensionless parameters are shown in Fig. 3b.

Figure 4 shows the aeroelastic stability boundary for the reference laminate with sweep angles of 10 and 30 deg. The boundary is shown as normalized dynamic pressure, which is defined as

$$q^*=\frac{q}{q_{\text{ref}}}=\frac{D_{11}\tilde{q}/\cos^2\Lambda}{(D_{11}\tilde{q}/\cos^2\Lambda)_{\text{ref}}} \tag{22}$$

where the reference condition is $\Lambda=0$, $\theta=0$. For the 10-deg swept wing, divergence is the mode of instability when ψ is positive and the ply angle is between -10 and -40 deg. As the sweep angle increases, the range of fiber angles during which divergence is seen decreases. By the time a 20-deg sweep angle is reached, divergence is no longer a part of the boundary for any of the values of ψ studied, as shown by the curve for the 30-deg swept wing.

Aeroelastic Tailoring

Most modern commerical aircraft are operating with aspect ratios in the range of 8–10, and their primary structure is aluminum. The next generation of such transport aircraft will make much more use of composite materials in their primary structure and will be able to be designed with considerably higher aspect ratios. The study by Jensen et al.[4] gives a number of designs optimized for various goals for which the aspect ratios go up to 15 and wing sweep angles range between 10 and 40 deg.

One of the limitations on the maximum aspect ratio of a wing is structural, and the use of a composite wing structure offers advantages from both the structural and aeroelastic viewpoints. Since the flutter speed of an aircraft decreases as the aspect ratio increases, in order to use the proposed high aspect ratios, the use of composites is mandated. By tailoring the laminate, it is possible to raise the flutter dynamic pressure over the equivalent quasi-isotropic value. Although it is not possible to eliminate the problem of flutter, the point may be reached where the aeroelastic benefits of increasing the flutter speed are offset by lowering the bending stiffness of the wing.

The results could be divided into two categories: low sweep angles (0 and 10 deg), which showed the occurrence of divergence in the presence of strong bending-torsion coupling; and moderate sweep angles (greater than 20 deg), for which 30 deg was chosen as representative. These configurations were chosen to represent the high-aspect-ratio wings that may be used for future transport aircraft.

Symmetric Laminates

Twenty-four plies are used in all configurations, and the laminate code is

$$[\theta_1,\theta_2,\theta_3,0,\mp 45,0,\mp 45,0,\mp 45]_s \tag{23}$$

In the previous section, the tailoring was achieved by orienting plies θ_1 and θ_2 at the reference angle, and the results were not surprising, showing the optimum fiber angle to be around -45 deg for cases in which divergence was not a problem and 45 deg when divergence was indicated. In order to see if any improvement could be obtained, and if there were any laminates that should be avoided, some alternate patterns were tried.

Some improvement was seen when θ_2 was the reverse of θ_1, and this was due to the elimination of bending-torsion coupling. Figure 5 shows the aeroelastic boundary and

Table 1 Dimensionless flutter pressure and relative computational time for reference case

Number of nodes	Straight wing	Tapered wing	Relative CPU time
3	3.7312	32.537	0.57
4	3.8489	35.674	1.00
5	3.8591	28.738	1.57
6	3.8582	28.366	2.56

Table 2 Properties of the reference case

Structural:	Aerodynamic:
Material: AS/3501 graphite epoxy	Aspect ratio = 14
Number of layers: 24	$c_{l\alpha}=5.0$
$e=-0.34$	a.c. $=-0.25$
	$\mu=11.1$
Inertial:	
$m_\alpha=1.0$	
$\chi_\alpha=0.2$	
$r_\alpha=0.538$	

dimensionless modulus parameters for this layup. Comparison with the curves in Fig. 4 shows that divergence has been prevented, and the flutter boundary has been raised by about 10%, this case when the outer plies are laid up at ±45 deg. Divergence is avoided in this case because the coupling parameter ψ is close to zero.

Further improvement was found when the third lamina was also varied, and Fig. 6a shows the stability boundary for this case with $\theta_2 = \theta_1$ and $\theta_3 = -\theta_1$. There is considerable improvement due to the increase in torsional stiffness. The maximum value of R is raised by about 30%, but since the laminate is no longer balanced there is some bending-torsion coupling. The increase in R raises the maximum flutter speed by 27% for the 30-deg swept wing and by 22% for the unswept case. Since there is strong coupling, divergence reappears for the unswept case when ψ is negative.

Clearly, this trend could be continued, ending with a laminate consisting of only ±45° laminae. This would, however, result in a wing that is very weak in bending, which would not meet strength requirements. Thus, the designer must reach a balance between the necessary bending stiffness and the aeroelastic constraints.

General Laminates

Symmetric laminates have several advantages over general, or nonsymmetric, laminates. First, there is no warping of the laminate and, second, they are easier to analyze and offer fewer design decisions. However, general laminates should not be ignored simply because they complicate the problem; indeed, they give the designer the fullest benefit of an anisotropic material. Warping may be most problematical if flat panels are needed, since the warping may put initial stress in the laminate. It may be possible to reduce this by curing a nonsymmetric laminate in subsections, which are themselves symmetric, and then bonding these subsections together after the initial cure cycle. If, however, the panel needs to be curved, such as may be the case for an aircraft wing, then using a nonsymmetric laminate may offer the means to such curvature.

A number of nonsymmetric laminates were examined, all having the following laminate code:

$$[\theta_1,\theta_2,0,0,\mp 45,0,\mp 45,0,\mp 45,\pm 45,0,\pm 45,0,\pm 45,0,0,\theta_{23},\theta_{24}]_T \tag{24}$$

For general laminates, two additional moduli, ψ_1 and ψ_2, are needed to define the structural behavior of the wing. A laminate that has a ply at angle θ below the midplane and one with the same angle, positive or negative, at the same distance above the midplane is said to be balanced, and $B_{11} = \psi_1 = 0$.

Figure 7 shows the stability boundary and modulus curves for a balanced nonsymmetric laminate, which is obtained by setting

$$\theta_1 = \theta_2 = -\theta, \qquad \theta_{23} = \theta_{24} = \theta \tag{25}$$

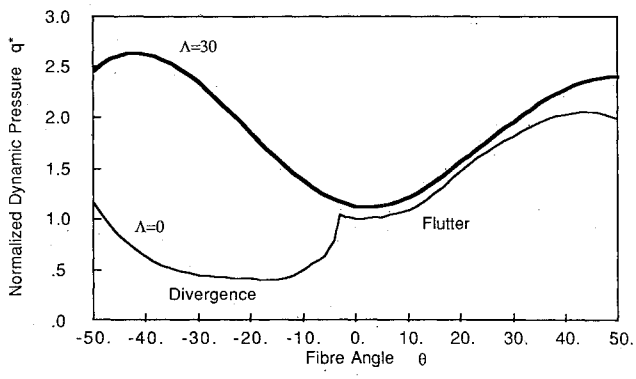

Fig. 6a Aeroelastic boundary for $\theta_2 = \theta_1 = \theta$ and $\theta_3 = -\theta$.

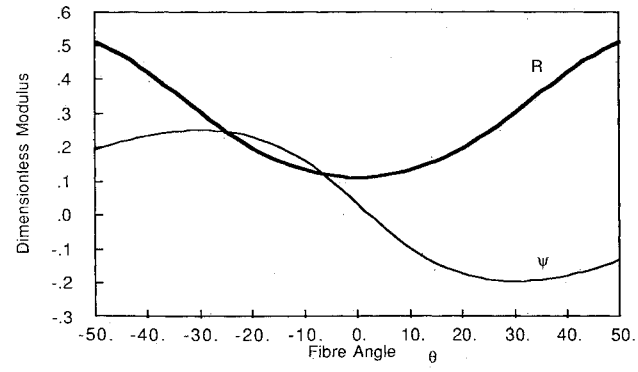

Fig. 6b Dimensionless modulus parameters R and ψ for $\theta_2 = \theta_1 = \theta$ and $\theta_3 = -\theta$..

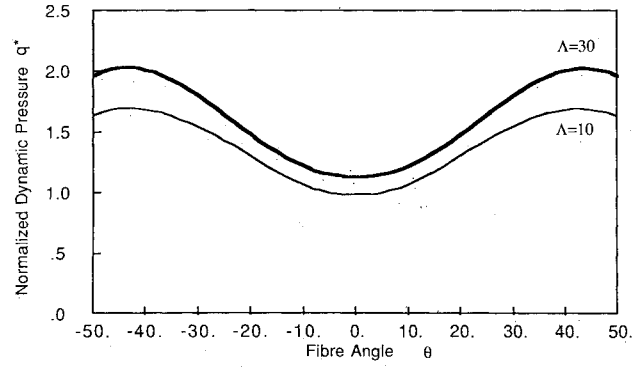

Fig. 7a Aeroelastic boundary for balanced general laminate: $\theta_1 = \theta_2 = -\theta$ and $\theta_{23} = \theta_{24} = \theta$.

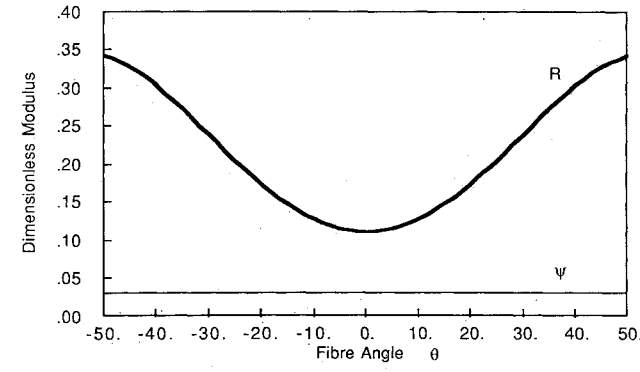

Fig. 7b Dimensionless modulus parameters R and ψ.

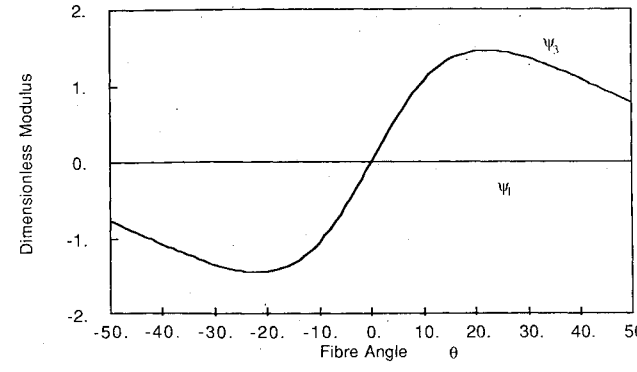

Fig. 7c Dimensionless modulus parameters ψ_1 and ψ_3.

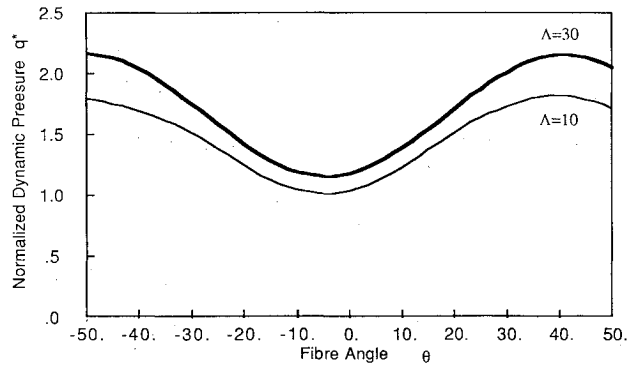

Fig. 8a Aeroelastic boundary for unbalanced general laminate: $\theta_1 = \theta + 10$ deg, $\theta_2 = \theta - 10$ deg, $\theta_{23} = -\theta$, and $\theta_{24} = \theta$.

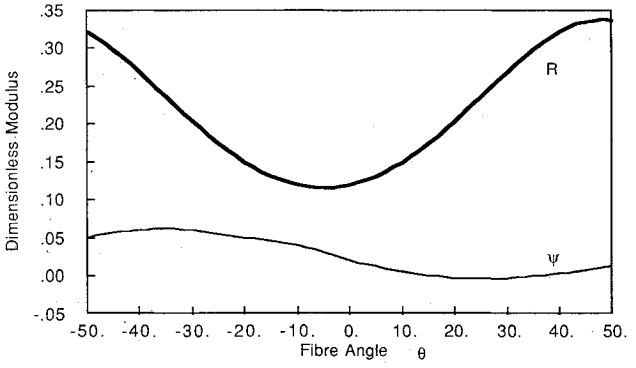

Fig. 8b Dimensionless modulus parameters R and ψ.

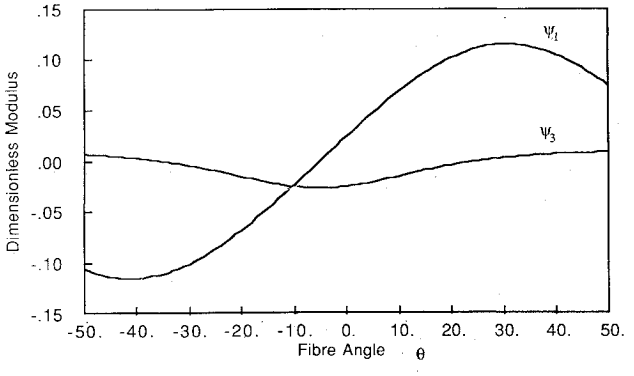

Fig. 8c Dimensionless modulus parameters ψ_1 and ψ_3.

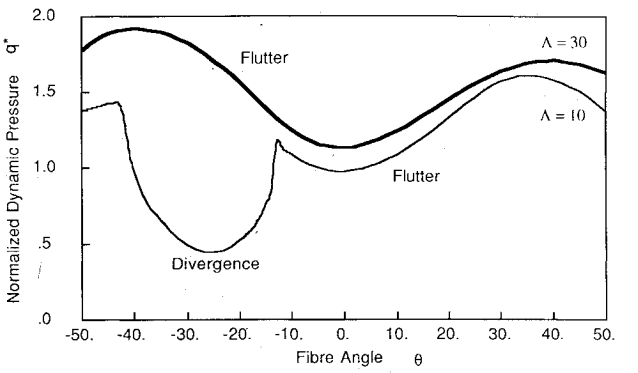

Fig. 9a Aeroelastic boundary for unbalanced general laminate: $\theta_1 = \theta_2 = \theta + 10$ deg and $\theta_{23} = \theta_{24} = \theta$.

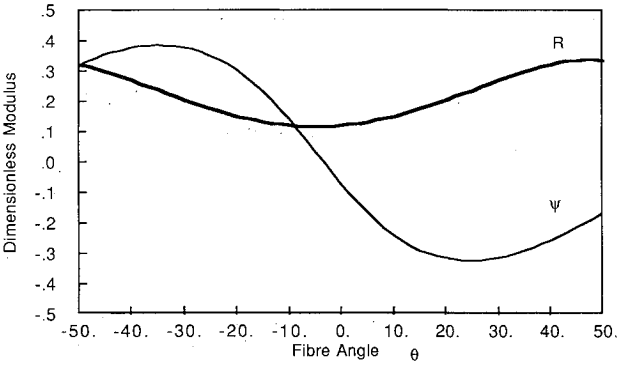

Fig. 9b Dimensionless modulus parameters R and ψ.

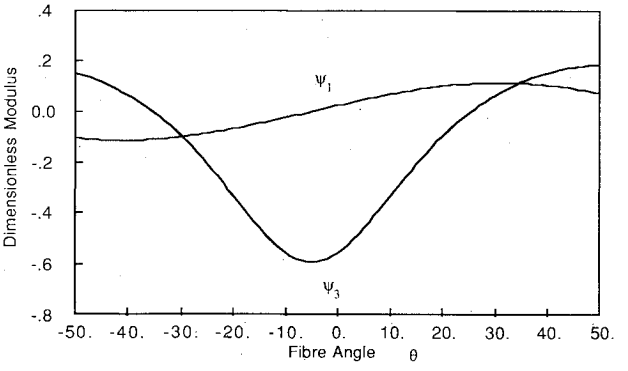

Fig. 9c Dimensionless modulus parameters ψ_1 and ψ_3.

There is also little bending-torsion coupling, $\psi \approx 0$, but there is strong extension-torsion coupling. R and ψ are almost the same as in Fig. 5b, but the flutter maximum is lowered by about 7%. The results are still better than the reference laminate, but there is a penalty for having extension-torsion coupling.

The next laminate examined had the following layup:

$$\theta_1 = \theta + 10 \text{ deg}, \quad \theta_2 = \theta - 10 \text{ deg}, \quad \theta_{23} = -\theta, \quad \theta_{24} = \theta \qquad (26)$$

which had the effect of eliminating ψ and ψ_3 but allowing extension-bending coupling. The effect on the flutter boundary, as shown in Fig. 8, was to improve it to the point where the maximum flutter pressure was about the same as that of the symmetric laminate shown in Fig. 5a and better than the balanced laminate of Fig. 7a.

As a final example, a completely general laminate was examined for which all three coupling parameters were nonzero. The laminate used is described by

$$\theta_1 = \theta_2 = \theta + 10 \text{ deg}, \qquad \theta_{23} = \theta_{24} = \theta \qquad (27)$$

and the results are shown in Fig. 9. Since ψ is no longer zero, the 10-deg swept wing is again prone to divergence, and the maximum flutter pressures are almost the same as those for the reference laminate. Again, there is some penalty for allowing coupling, but it need not completely prevent general laminates from being considered. The penalty for this case is partly due to the extensional coupling and partly to the reappearance of bending-torsion coupling.

Conclusions

The aim of this analysis was to examine the usefulness of the integrating matrix method for the study of the aeroelastic stability for fairly arbitrary geometries and to examine the possibilities of using general, nonsymmetric laminates. Although it is possible to incorporate refinements into the integrating matrix method, such as including three-dimensional aerodynamic effects, this work emphasizes its use as a preliminary design tool to study a broad range of laminates. Adding refinements to the method is necessary when making comparisons with experiment, but such additions increase

the cost of solution and are unlikely to change the trends presented.

Most studies in aeroelastic tailoring have considered only symmetric laminates, but it is of interest to study the effect of using general laminates. Nonsymmetric laminates introduce two additional coupling parameters to the problem, and three general laminates were examined to reflect the contribution of each of these on the stability. Extension-torsion coupling, ψ_3, caused some degradation of the flutter boundary; extension-bending coupling, ψ_1, was not as damaging as ψ_3 and gave a flutter boundary that was as good as the best symmetric laminate with the same torsion-bending stiffness ratio. When both ψ_1 and ψ_3 were present, the performance of the wing was degraded to that of the symmetric reference laminate. It is worth noting that such nonsymmetric laminates may be more applicable to helicopters, where there is an extensional force due to rotation that may be beneficially combined with the extensional coupling parameters.

It was possible only to show the results for a limited number of laminates, and those shown were among the better layups investigated. If general laminates are to be used, there are even more permutations to add to the designer's problem. However, this preliminary investigation shows that there need not be a severe penalty for making use of a general laminate—this is a topic worthy of further research.

Acknowledgment

This research was supported by the National Aeronautics and Space Administration under Grant NGL 05-020-243.

References

[1]Shirk, M. H., Hertz, T. J., and Weisshaar, T. A., "Aeroelastic Tailoring—Theory, Practice and Promise," *Journal of Aircraft*, Vol. 23, Jan. 1986, pp. 6–18.

[2]Krone, N. J., "Divergence Elimination with Advanced Composites," AIAA Paper 75-1009, Aug. 1975.

[3]Weisshaar, T. A. and Ryan, R. J., "Control of Aeroelastic Instabilities through Stiffness Cross Coupling," *Journal of Aircraft*, Vol. 23, Feb. 1986, pp. 148–155.

[4]Jensen, S. C., Rettie, I. H., and Barber, E. A., "Role of Figures of Merit in Design Optimization and Technology Assessment," *Journal of Aircraft*, Vol. 18, Feb. 1981, pp. 76–81.

[5]Gimmestad, D., "An Aeroelastic Optimization Procedure for Composite High Aspect Ratio Wings," *Proceedings of the 20th AIAA/ASME/ASCE/AHS Structures, Structural Dynamics, and Materials Conference*, Vol. 1, St. Louis, MO, April 1979, pp. 79–86.

[6]Lehman, L. L., "A Hybrid State Vector Approach to Aeroelastic Analysis," *AIAA Journal*, Vol. 20, Oct. 1982, pp. 1442–1449.

[7]Lehman, L. L., "Hybrid State Vector Methods for Structural Dynamic and Aeroelastic Boundary Value Problems," Ph.D. thesis, Stanford University, Stanford, CA, Feb. 1982.

[8]Green, J. A., "Aeroelastic Tailoring of Composite Wings with External Stores," *Proceedings of the 27th AIAA/ASME/ASCE/AHS Structures, Structural Dynamics, and Materials Conference*, Vol. 1, San Antonio, TX, May 1986, pp. 710–719.

[9]Tsai, S. W. and Hahn, H. T., *Introduction to Composite Materials*, Technomic Publishing, Westport, CT, 1980.

[10]Librescu, L. and Simovich, J., "A General Formulation for the Aeroelastic Divergence of Composite Swept Forward Wing Structures," *Proceedings of the 15th Congress of the International Council of the Aeronautical Sciences*, London, England, Sept. 1986, pp. 1129–1140.

[11]Yates, E. C. Jr., "Flutter and Unsteady Lift Theory. Performance of Aerospace Vehicles," NASA SP 258, 1971, pp. 289–374.

[12]Weisshaar, T. A., Zeiler, T. A., Hertz, T. J., and Shirk, M. H., "Flutter of Forward Swept Wings, Analyses and Tests," *Proceedings of the 23rd AIAA/ASME/ASCE/AHS Structures, Structural Dynamics, and Materials Conference*, Vol. 2, New Orleans, LA, May 1982, pp. 111–121.

[13]Chen, G-S. and Dugundji, J., "Experimental Aeroelastic Behavior of Forward Swept Graphite/Epoxy Wings with Rigid Body Freedoms," *Proceedings of the 27th AIAA/ASME/ASCE/AHS Structures, Structural Dynamics, and Materials Conference*, Vol. 1, San Antonio, TX, May 1986, pp. 111–121.

[14]Conte, S. D. and deBoor, C., *Elementary Numerical Analysis. An Algorithmic Approach*, 2nd Ed., McGraw-Hill, New York, 1972.